Physics of Fluids

Flameless combustion of low calorific value gases, experiments, and simulations with advanced radiative heat transfer modeling

Cite as: Phys. Fluids **34**, 045123 (2022); https://doi.org/10.1063/5.0087077
Submitted: 01 February 2022 • Accepted: 06 April 2022 • Published Online: 25 April 2022

Phuc-Danh Nguyen, Huu-Tri Nguyen, Pascale Domingo, et al.

Physics of Fluids ARTICLE scitation.org/journal/phf

Flameless combustion of low calorific value gases, experiments, and simulations with advanced radiative heat transfer modeling

Cite as: Phys. Fluids **34**, 045123 (2022); doi: 10.1063/5.0087077
Submitted: 1 February 2022 · Accepted: 6 April 2022 ·
Published Online: 25 April 2022

Phuc-Danh Nguyen,[1,a)] Huu-Tri Nguyen,[1,2] Pascale Domingo,[2] Luc Vervisch,[2] Gabriel Mosca,[3] Moncef Gazdallah,[4] Paul Lybaert,[4] and Véronique Feldheim[4]

AFFILIATIONS

[1]ArcelorMittal Global Research and Development, Maizières Process, Voie Romaine, BP 30320, 57283 Maizières-lès-Metz Cedex, France
[2]CORIA-CNRS, Normandie Université, INSA Rouen Normandie, 76801 Saint-Etienne-du-Rouvray, France
[3]BuildWind, Rue Bara 175, 1070 Brussels, Belgium
[4]Université de Mons, Service de Thermique et Combustion, Rue de l'Epargne 56, 7000 Mons, Belgium

Note: This paper is part of the special topic, Development and Validation of Models for Turbulent Reacting Flows.
[a)]**Author to whom correspondence should be addressed:** phucdanh.nguyen@arcelormittal.com

ABSTRACT

Thermal radiation is the dominant mode of heat transfer in many combustion systems, and in typical flameless furnaces, it can represent up to 80% of the total heat transfer. Accurate modeling of radiative heat transfer is, thus, crucial in the design of these large-scale combustion systems. Thermal radiation impacts the thermochemistry, thereby the energy efficiency and the temperature sensitive species prediction, such as NO_x and soot. The requirement to accurately describe the spectral dependence of gaseous radiative properties of combustion products interacts with the modeling of finite rate chemistry effects and conjugates heat transfer and turbulence. Additionally, because of the multiple injection of fuels and/or oxidizers of various compositions, case-specific radiative properties' expressions are required. Along these lines, a comprehensive modeling to couple radiation and combustion in reacting flows is attempted and applied to the simulation of flameless combustion. Radiation is modeled using the spectral line-based weighted-sum-of-gray-gases approach to calculate gaseous radiative properties of combustion products using the correlation of the line-by-line spectra of H_2O and CO_2. The emissivity weights and absorption coefficients were optimized for a range of optical thicknesses and temperatures encountered in the considered furnace. Efforts were also made on the development of a reliable and detailed experimental dataset for validation. Measurements are performed in a low calorific value syngas furnace operating under flameless combustion. This test rig features a thermal charge which can extract about 60% of combustion heat release via 80% of radiative heat transfer, making it of special interest for modeling validation. The comparison between the simulation and the experiment demonstrated a fair prediction of heat transfer, energy balance, temperature, and chemical species fields.

I. INTRODUCTION

With increasing energy cost, natural resources limitation of fossil fuels, and more stringent regulation on CO_2 and pollutant emissions, it is mandatory to look for alternative low-carbon fuels and to develop more energy efficient and cleaner combustion systems. Industrial auto-produced low calorific value (LCV) fuel gases constitute a promising alternative energy source combined with advanced combustion technologies. Diluted, flameless, or "MILD" combustion[1–3] is one of the best candidates that fulfill the requirements in terms of improved combustion efficiency, low emissions of soot and NO_x, and fuel flexibility. Such a flameless or MILD combustion mode is obtained by the dilution of reactants with combustion products before the reactants are mixed so that the reaction rates are slow, and the reaction occurs in a larger volume compared to a classical flame combustion. The success in the design of such advanced combustion applications relies heavily on accurate and efficient coupled combustion and radiation modeling, which also requires a reliable and detailed experimental database for validation. Today, multiple injection of fuels and/or oxidizers can feature in a single furnace to allow for flexible energy source utilization and for CO_2 mitigation, and this requires the development

of case-specific radiative properties modeling. Along this line, radiation modeling based on the spectral line-based weighted-sum-of-gray-gases (SLWSGG) approach[4–8] was proposed to build a comprehensive multi-physics CFD model, which is applied to simulate a flameless combustion furnace. All of these are in the framework of RANS simulation.

The gaseous radiative properties of combustion products are calculated using the correlation of the line-by-line spectra of H_2O and CO_2.[9–15] The emissivity weights and absorption coefficients were evaluated and optimized for a range of optical thicknesses and temperatures encountered in the furnace under consideration. An experimental database of flameless combustion of a LCV syngas on a lab-scale furnace was built specifically for the validation of the proposed comprehensive modeling methodology.

Experimental study of flameless combustion for high calorific value (HCV) gases, such as methane or hydrogen, can be found in the literature; jet-in-hot-coflow burners,[16] Delft lab-scale furnace,[17] or MILD combustion of methane/hydrogen mixtures[18] can be cited as a few. There was often the absence of a strong heat sink to reproduce important radiative heat transfer as observed in large-scale combustion systems. It is also noticed that there was lack of discussion on experimental databases regarding LCV gases in the literature. Along these lines, a lab-scale furnace designed to stabilize flameless combustion of a LCV syngas is proposed in the present study, and the experimental database serves to validate the developed modeling. Main relevant features of flameless combustion as observed in the industrial context are mimicked: strong entrainment of burnt gases by the aerodynamics of high velocity reactant jets to promote highly diluted combustion, air preheated to very high temperature up to 1000 °C to reproduce air preheating with regenerative burner technology, and the presence of the strong heat sink (cooling tubes) to simulate important radiative heat transfer from combustion to thermal charge. Combustion of natural gas with air was first studied[19–21] in the same test rig, and then the gas injector was redesigned to stabilize flameless combustion of a LCV syngas, a co-product gas produced in the steel industry.[22,23] Flameless combustion was then characterized with detailed in-furnace measurements of temperatures and chemical species.

In the test rig of the present study, the thermal charge extracts about 60% of combustion heat release, 80% of which by radiative heat transfer, and 20% by convection. Radiative heat transfer is clearly the dominant mode of heat transfer as observed in large-scale combustion systems. This makes the test rig a special interest with detailed in-furnace measurements for validation of radiation and/or combustion models.

Many difficulties arise when dealing with radiation modeling: Highly spectral dependence of gaseous radiative properties, large CPU cost going with the solving of the radiative transfer equation (RTE), and consideration of finite rate chemistry for highly diluted combustion can be cited among others.[24,25] In a recent review paper, Liu *et al.*[25] outlined the challenges associated with radiative transfer predictions in combustion applications and the different approaches that may be used with tradeoffs. The SLWSGG model has the advantages and the capability to extend to modeling large-scale industrial furnaces, featuring multi-injection of low-carbon fuels and/or oxidizers in different zones for decarbonization. Because of various compositions and conditions, case-specific radiative properties' expressions are required. The SLWSGG model appears to be the best choice, and most adapted for that purpose while keeping a compromise between accuracy and CPU cost. If we focus on the radiation aspect, it is noted that efforts were spent mainly on the modeling of gaseous radiative properties for HCV gases such as natural gas, and there is a lack of discussion on radiation modeling of LCV gases.

Radiation modeling based on the spectral line-based weighted-sum-of-gray-gases (SLWSGG) approach[4,5,8] is proposed to calculate radiative properties of combustion products of different fuel gases with application to the combustion of a LCV syngas. The parameters in the SLWSGG model are obtained from the correlation of the line-by-line spectra of H_2O and CO_2.[9–15] In fact, together with the absorption distribution function (ADF)[26] and statistical narrow band full spectrum correlated K (SNB-FSCK)[27] models, the SLWSGG model belongs to the non-gray global model family, which has a special interest for complex combustion system simulations for two reasons: First, it is more accurate than the simple gray gas model, and second, it is more computationally efficient than the statistical narrow band correlated K (SNB-CK) model.[28] The SLWSGG approach is also straightforward to incorporate into the widely used discrete ordinate method (DOM)[29] to discretize the radiative transfer equation (RTE), thus ensuring a good compromise between solution accuracy over a wide range of optical thicknesses and computational cost.[30] Three gray gases were considered in the study to mitigate the CPU time.[31,32] The emissivity weights and absorption coefficients of the syngas combustion products were evaluated and optimized over a range of optical thicknesses and temperatures encountered in the considered test rig. The radiative properties were integrated into the Ansys Fluent® flow solver[33] using user defined functions for a full coupling of combustion and radiation.

Section II describes briefly the experimental setup and numerical modeling approach. The results will be presented in Sec. III. Finally, some concluding remarks will be formulated in the conclusion.

II. EXPERIMENTATION AND NUMERICAL MODELING

A. Experimental setup and measurement

Figure 1 shows a picture of the flameless combustion furnace[19–23] with its schematic and dimensions of the burner section. The combustion chamber is made of stainless steel and equipped with a fibrous ceramic heat insulation layer. It has a square inner section of 0.35 × 0.35 m^2 with 1.0 m high. One air injection with 24.8 mm exit diameter is located in the center. Two gas injectors with 11° tilt angle are symmetrically located around the air injector. The diameter of the fuel gas injector was designed to stabilize flameless combustion. The air was preheated up to 800 °C by an electrical preheater. The fuel gas compositions are realized using a mixing unit equipped with mass flow meters and controllers fed through pure gas bottles. The thermal charge and the furnace temperature are controlled through four water cooling tubes (heat sink), and the immersion of which can be regulated from 0 to 90 cm and a reduced water circuit along the outer walls. Each vertical wall of the combustion chamber has a removable part. A wall [on the rear side of Fig. 1(a)] is equipped with a quartz window to allow for optical access and image recording. A LaVision intensified camera with an UV filter centered at 329 nm is used to take images of chemiluminescent self-emission of OH^* radicals at 308 nm wavelength.[34] OH^* imaging allowed for determining the position of main reaction zones. A sidewall [on the right of Fig. 1(a)] is equipped with eight S-type thermocouples, 0.09 m separated each other and mounted flush with the insulation layer in order to get a wall temperature profile

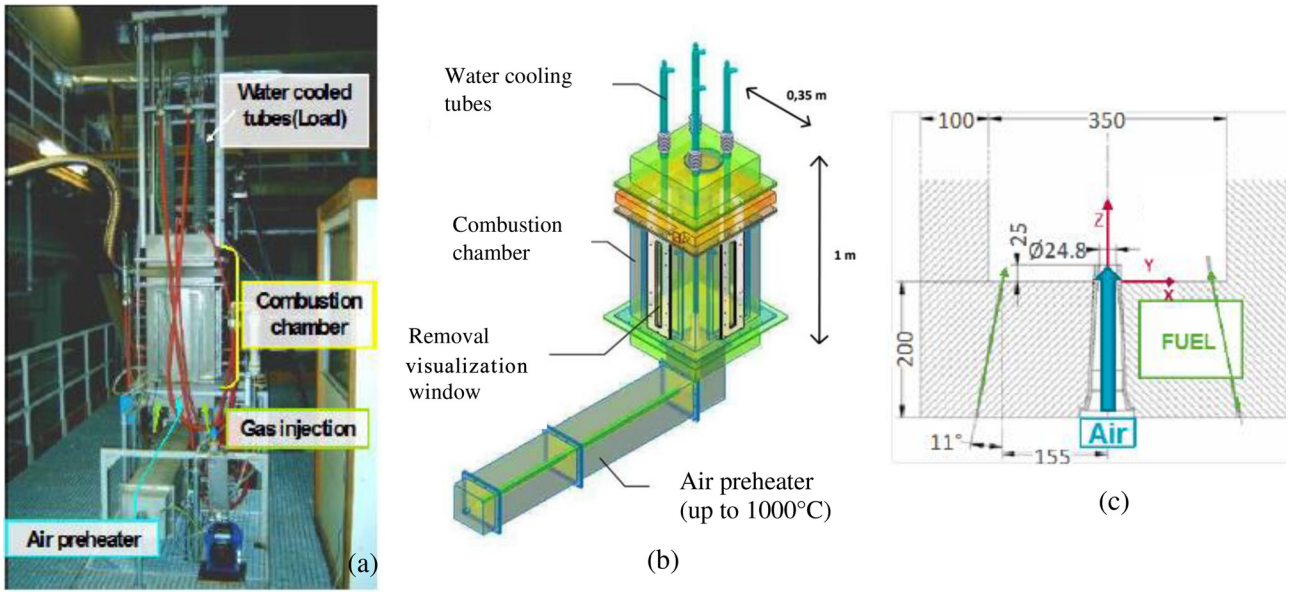

FIG. 1. (a) Picture of the flameless combustion furnace, (b) its schematic representation, and (c) the dimensions in mm of the burner section.

along the furnace height in the vertical symmetry plane containing the air and gas injectors. The measurements of the temperature and species concentration at the furnace exit and inside the furnace were realized by the two home-made probes, which are inserted inside the furnace through 14 holes on the wall opposite to the thermocouples wall. The suction pyrometer probe is equipped with a S-type thermocouple and works with a Venturi's tube connected to an air compressed circuit. The gas sampling probe is equipped with a vacuum pump to extract burnt gases with a flow rate equal to 210 Nl/h. Water is removed, and the dry sample is sent in parallel to the chromatograph and gas analyzers. The concentrations of O_2, CH_4, CO_2, and CO (on dry basis) were measured by the paramagnetic and infrared gas analyzers. Measurement of H_2 and N_2 and another measurement of O_2, CH_4, and CO were realized by the gas chromatograph. More details regarding the experimental procedure and measurements can be found in our previous works.[19–23] The studied syngas composition is (by volume): 32.5%H_2, 14.25%CH_4, 13.25%CO, 12%CO_2, and 28%N_2. A flameless combustion regime was established at 30 kW of fuel power.

B. Numerical modeling and simulation

In the concept of the weighted-sum-of-gray-gases (WSGG) model, the non-gray gas is replaced by an equivalent number of gray gases with different absorption coefficients and emissivity,[35] for which the heat transfer rates are calculated independently. The total heat flux is then calculated by adding the heat fluxes of each gray gas. The WSGG concept was extended to consider spectral lines information called the spectral line-based weighted-sum-of-gray-gases (SLWSGG) model.[4,5,8] The SLWSGG model is applied in its very fine integration form. However, it should be noted that Webb *et al.*[36] and Badger *et al.*[24] proposed the most recent implementation of the model named the rank correlated SLW model, which can produce accurate results with as few as three gray gases requiring no optimization. The detailed theoretical background of such models can be found in the book of Modest.[27] Only a brief description of the concept is given. The radiative transfer equation (RTE) to be solved is

$$\frac{dI_i}{ds} = k_i p_a (a_i I_b - I_i), \tag{1}$$

where I_i(W/m) is the radiation intensity along the direction s of the ith gray gas, I_b (W/m) is the blackbody radiation intensity, k_i(m^{-1} atm^{-1}) is the pressure-based absorption coefficient of the ith gray gas, p_a (atm) is the sum of the partial pressures of the absorbing species, and a_i is the emissivity weighting factor of the ith gray gas with temperature dependence. The RTE is solved for each gray gas $i = 1, 2, \ldots, N$ (N is the total number of gray gas) with the boundary condition given by

$$s = 0 : I_i = \varepsilon_w a_i I_b(T_w) + \frac{1-\varepsilon_w}{2\pi} \int_{\vec{s}\vec{n}<0} I_i d\omega \tag{2}$$

(ε_w and T_w are the wall emissivity and wall temperature, respectively) using the discrete ordinate method (DOM).[29] The emissivity weighting factors and absorption coefficients are evaluated and optimized over a range of optical thicknesses and temperatures encountered in the considered domain. Total emissivity is calculated from the contribution of all gray gas emissivities as such

$$\varepsilon(T, L, p_a) = \sum_{i=0}^{N} a_i (1 - e^{-k_i p_a L}), \tag{3}$$

where T(K) is the gas temperature and L(m) is the optical thickness. Each gray gas is characterized by an emissivity weighting factor and an absorption coefficient, which can be described by temperature dependent polynomials of $J-1$ degree written in the form of

$$a_i = \sum_{j=1}^{J} \alpha_{i,j} T^{j-1}, \tag{4}$$

$$k_i = \sum_{j=1}^{J} \beta_{i,j} T^{j-1}, \tag{5}$$

where $\alpha_{i,j}$ and $\beta_{i,j}$ denote the polynomial coefficients for the emissivity weighting factor and the absorption coefficient, respectively. For transparent regions of the spectrum (clear gas $i = 0$), the absorption coefficient is set to zero ($k_0 = 0$) in order to account for windows in the spectrum between spectral regions of high absorptions, and the clear gas emissivity weighting factor is $a_0 = 1 - \sum_{i=1}^{N} a_i$.

The polynomial coefficients $\alpha_{i,j}$ and $\beta_{i,j}$ of Eqs. (4) and (5) are determined and optimized following the steps:

(i) For a given molar fraction of H_2O and CO_2, a range of optical thicknesses encountered in the considered domain and a fixed temperature T, the SLWSGG model with 30 gray gases is used to calculate the "true" emissivity curves $\varepsilon(T, p_a L)$. In the SLWSGG model, the absorption distribution function is computed using the correlations proposed by Modest and Mehta[14] and Modest and Singh[15] for the cumulative full-spectrum k-distribution functions of H_2O and CO_2. The true emissivity weighting factor a_i is calculated by the difference of the absorption line blackbody distribution function F evaluated at the two bounds $(i,\ i-1)$ of the gray gas interval

$$a_i = F(C_{abs,i}, T_g, T_b, X_s, P) - F(C_{abs,i-1}, T_g, T_b, X_s, P), \tag{6}$$

$$F(C_{abs,i}, T_g, T_b, X_s, P) = \frac{\pi}{\sigma T^4} \sum_{m=0}^{\infty} \int_{\eta_m}^{\eta_{m+1}=\eta_m+\Delta\eta} g_m(C_{abs,i}, \eta, T_g, X_s, P)\, I_{b,\eta}(T_b, \eta)\, d_\eta, \tag{7}$$

where $C_{abs,i}, T_g, T_b, X_s$, P, and η are the absorption cross-sectional area $(m^2/mole)$, the gas temperature (K), the black body temperature (K), the species mole fraction, the absolute pression (bar), and the wave number (m^{-1}), respectively. The absorption coefficient k_i is related with the absorption cross-sectional area by $k_i = C_{abs,i} N_{mole}$ with N_{mole} being the mole density. The cumulative full-spectrum k-distribution functions g_m for H_2O and CO_2 using spectral correlations proposed by Modest and Mehta[14] and Modest and Singh[15] are given by

$$g_m = \frac{1}{2}\tanh\left[P_m(T_g, T_b, X_s, P; k)\right] + \frac{1}{2}, \tag{8}$$

where

$$P_m = \sum_{l=0}^{3}\sum_{m=0}^{3}\sum_{n=0}^{3} a_{lmn} \left[\frac{T_g}{1000}\right]^n \left[\frac{T_b}{1000}\right]^m \left[\log_{10} k\right]^l. \tag{9}$$

The correlation forms are similar for H_2O and CO_2, but the coefficients for the full-spectrum k-distribution a_{lmn} of H_2O and CO_2 are different and given in the studies of Modest and Mehta[14] and Modest and Singh.[15]

(ii) A least square method is used to calculate the absorption a_i and weight k_i coefficients for a fixed gray gas number N (N = 3 in our case), which best fit the "true" emissivity curve.

(iii) Steps (i) and (ii) are repeated for a set of M temperature points ranging from 300 to 1700 K as encountered in the considered domain.

(iv) The profiles of absorption and weight coefficients vs temperature obtained are used to calculate the polynomial coefficients.

Equations (4) and (5) were integrated into the Ansys Fluent flow solver[33] using user defined functions. The absorption coefficient and the emissivity weighting factor are updated before each solving of the RTE. The parameters of the model are obtained from the correlation of the line-by-line spectra of H_2O and CO_2.[9–15] The extension of the model to situations featuring multiple injection of fuels and/or oxidizers is straightforward. The number of gray gases N = 3 or 4 was found to be adequate for good quality of emissivity fittings, and further increase in the gray gases number did not lead to consistent improvement in accuracy.[31,32] Three gray gases were then considered in the study to keep CPU time and memory requirements acceptable. The DOM method[29] was used for angular discretization of RTE with nine solid angles per octant (3×3). DOM was chosen, because it is sufficiently accurate and applicable across a wide range of optical thicknesses, which is not well known in flameless combustion.[37]

The CFD solution is obtained numerically by solving RANS equations in steady state. The choice of the $k-\varepsilon$ RNG turbulence model[38] for this study is recommended from the study on the same furnace of Lupant,[20,21] who carried out a deep analysis of the effect of different turbulence models (of the two families $k-\varepsilon$ and $k-\omega$) considering the species distribution in a non-reacting mixture, to validate the turbulence model independently from the combustion model. The $k-\varepsilon$ RNG model developed for strained flows is found appropriate to predict the turbulent flowfield in the flameless combustion characterized by intense recirculation. The turbulence-chemistry interaction was modeled using the eddy-dissipation concept (EDC)[39,40] to consider finite chemistry effects. The chemical kinetics scheme KEE58[41] including 18 species and 58 elementary reversible reactions was used. A transport equation for each of these chemical species is solved except for nitrogen. The EDC model was used in its standard form even though some improvement for temperature prediction can be obtained by modifying or calculating directly volume fraction and residence time constants of species in fine structures based on local flow characteristics.[42–45] However, in the recent study of Silei *et al.*[46] for the MILD combustion system, which is similar to that in the present study in the sense that the MILD condition is obtained by burner design to promote internal flue gas recirculation, the standard EDC model (with the KEE58 chemical scheme) provided satisfied prediction while the EDC models with modified or locally calculated model constants did not show effective improvement. The flameless condition in the current study is different from that of jet-in-hot-coflow flames for which EDC constant modifications were proposed.[42–44]

The *in situ* adaptive tabulation (ISAT)[47] was used to accelerate the chemistry integration. The KEE58 scheme was validated for MILD combustion for various mixtures of H_2 and CH_4.[43,48,49] In Ref. 48, the KEE58 mechanism gave very similar results as compared to the GRI-3.0 detailed mechanism[50] in terms of mean temperature prediction, and the error is less than 5% in comparison with experiment. Prediction of NO formation in MILD combustion of CH_4–H_2 mixtures reasonably matched experimental values when post-processed from thermo-chemical field obtained with KEE58.[49] Also in Ref. 43,

KEE58 showed more reliable predictions than other schemes such as DRM-19 and DRM-22[51] in terms of temperature and species concentrations for MILD combustion of CH_4–H_2 mixtures. In the recent studies of Silei *et al.*[46] and Ferrarotti *et al.*[52] for the MILD and flameless combustion systems, which are similar to that in the present study, i.e., MILD or flameless conditions are obtained by burner designs to create internal flow recirculation, the KEE58 scheme provided satisfied predictions. It is also to notice that MILD combustion was studied in the framework of RANS modeling using EDC[42–45,48,49] or FGM (flamelet generated manifold)[53] to account for turbulence chemistry interaction.

The computational domain corresponds to the whole gas volume inside the furnace. The grid was made unstructured with nearly 6×10^6 hexahedral cells considering the grid independence study carried out in the same furnace operating on natural gas for a quarter of the domain thanks to symmetry.[20,21] The results showed that when the grid size increased from 640 thousand hexahedral cells to 1.3×10^6 hexahedral cells (equivalently 2.56×10^6 hexahedral cells to 5.2×10^6 hexahedral cells for the full domain in the present study), no more sensibility to grid size was observed for temperature and chemical species. $y^+ = 1$ on the walls of the air and gas injections while on the furnace walls y^+ is mainly around 15 and does not exceed 30. The resolution in the shear layer is $h = 7\,\mu m$. The boundary conditions were calibrated using the experimental measurements. Temperature, gas composition, and mass flow rates are fixed at inlets. For the other walls, the total heat loss (p_{loss}) from experimental heat balance is considered uniformly distributed on the walls with total surface (s_{wall}) and used to deduce a global heat transfer coefficient (k) between the inner wall temperature (T_{inn}) (average measured value) and the external environment temperature (T_{ext}). The expression for k is

$$k = \frac{P_{loss}}{s_{wall}\,(T_{inn} - T_{ext})}. \tag{10}$$

III. RESULTS OF NUMERICAL MODELING AND COMPARISON AGAINST THE MEASUREMENTS

A. Radiative properties SLWSGG modeling

The total emissivity was calculated and compared to the Hottel and Sarofim's database[35] as well as with the results obtained with Soufiani and Djavdan[54] and Smith *et al.*[55] methods for the available nearest configurations in terms of water vapor and carbon dioxide partial pressures. The SLWSGG used the correlation of the line-by-line spectra of H_2O and CO_2,[9–15] and the emissivity was evaluated and optimized over a range of optical thicknesses and temperatures encountered in the furnace. Figure 2 shows the emissivity of burnt gases issued from the stoichiometric combustion between the air and the studied syngas as well as the two other gases named COG (28.5%CH_4, 62%H_2, 6%CO, 1.5%CO_2, and 2%N_2 by volume), a HCV gas, and BFG (3%H_2, 20.5%CO, 22.5%CO_2, and 54%N_2 by volume), a

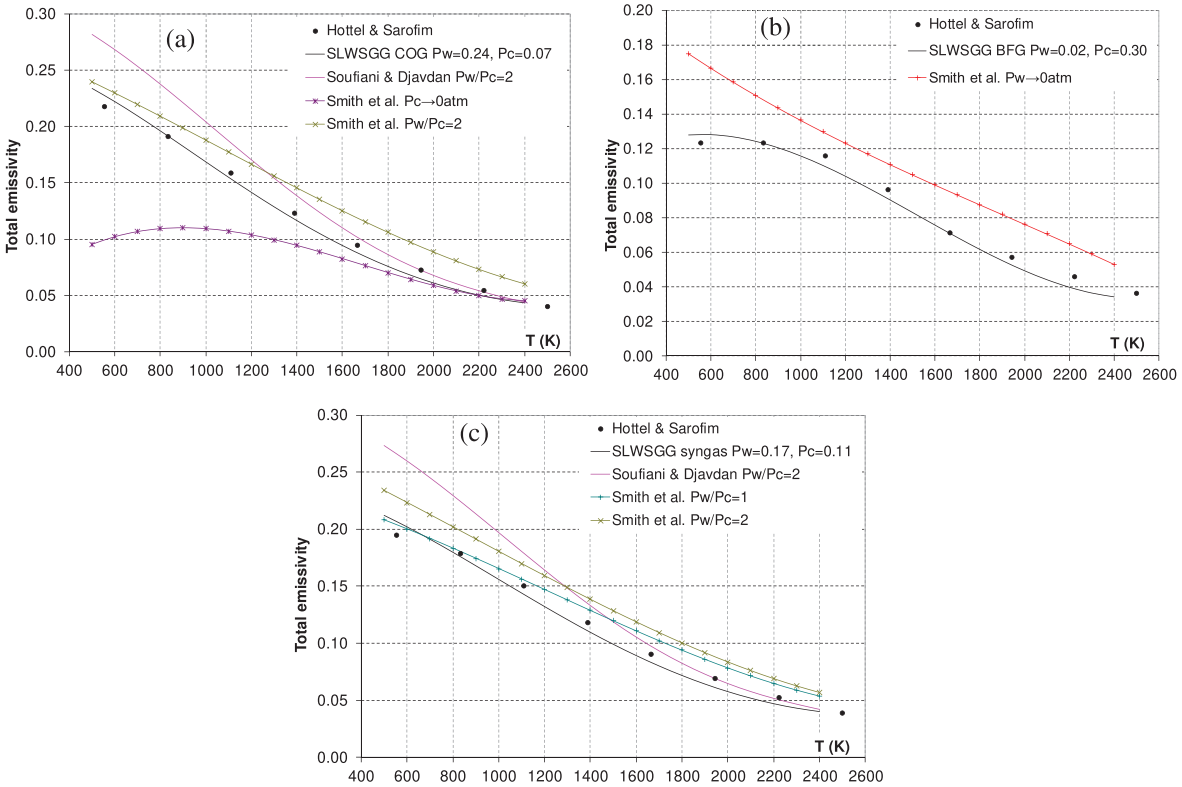

FIG. 2. Comparison of total emissivity calculated from different models for HCV COG (a), LCV BFG (b), and syngas (c). P_w and P_c are partial pressures of water vapor and carbon dioxide, respectively.

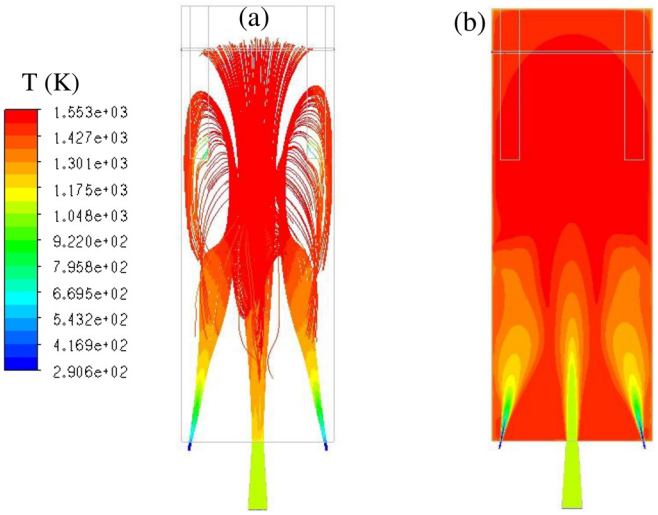

FIG. 3. (a) Pathlines of reactants jets colored by temperature. (b) Temperature contour obtained by CFD in the symmetrical plane.

LCV gas. The studied syngas is indeed composed of 50% of COG and 50% of BFG by volume.

The results shown in Fig. 2 were obtained using the averaged optical length of the studied geometry for all models and Hottel and Sarofim's database. The SLWSGG model results were obtained using three gray gases, and the same number of gray gases was used in the CFD simulations. Regarding the HCV case, as shown in Fig. 2(a), the SLWSGG model is closer to Hottel and Sarofim's database than the method of Soufiani and Djavdan[54] and Smith *et al.*;[55] the configuration $P_c \rightarrow 0$ atm of Smith *et al.*[55] showed an important departure from the Hottel and Sarofim's database. For the LCV case [Fig. 2(b)], the SLWSGG model agrees with Hottel and Sarofim's database while the total emissivity obtained with the $P_w \rightarrow 0$ atm configuration of Smith *et al.*[55] shows a departure from the Hottel and Sarofim's database. Finally concerning the syngas case [Fig. 2(c)], the SLWSGG also showed better performance. This confirms that the development of case-specific radiative properties' modeling is required to secure accurate prediction of radiative heat transfer particularly in combustion systems featuring multiple injection of HCV and LCV fuels for optimized energy sources utilization.

B. Characterization of flameless combustion

Flameless or MILD combustion is characterized by dilution of reactants with low enthalpy combustion products before the mixing between the reactants themselves so that the reaction rates are slow, and the reaction zone spreads over a much larger volume compared to a classical flame combustion. The dilution is obtained by a high flow recirculation induced by the aerodynamics of the high velocity reactants jets as shown by the pathlines of the reactants jets in Fig. 3(a). Figure 3(b) shows the temperature distribution obtained by simulation in the symmetrical plane. It is observed that the temperature distribution is quite homogeneous in the combustion zone with no local hot spots, confirming the flameless mode. The two lateral syngas jets emerge into the combustion chamber with a high velocity of nearly 100 m/s entraining the burnt gases and creating two important recirculation zones. In this condition, the air and fuel gas are highly diluted by the burnt gases.

Figure 4(a) presents the theoretical trajectory of the fuel jet, which is calculated based on the strong jet/weak jet (SJWJ) interaction theory developed by Grandmaison *et al.*[56] (only the left part of the furnace is presented for the sake of brevity). The line representing the air jet opening was also plotted in the same figure. The ordinate z of the SJWJ theory fuel trajectory is given by

$$z = \xi d_{12}, \tag{11}$$

$$\xi = -\int_1^{\eta} f^{-1} \cos\theta d\eta, \tag{12}$$

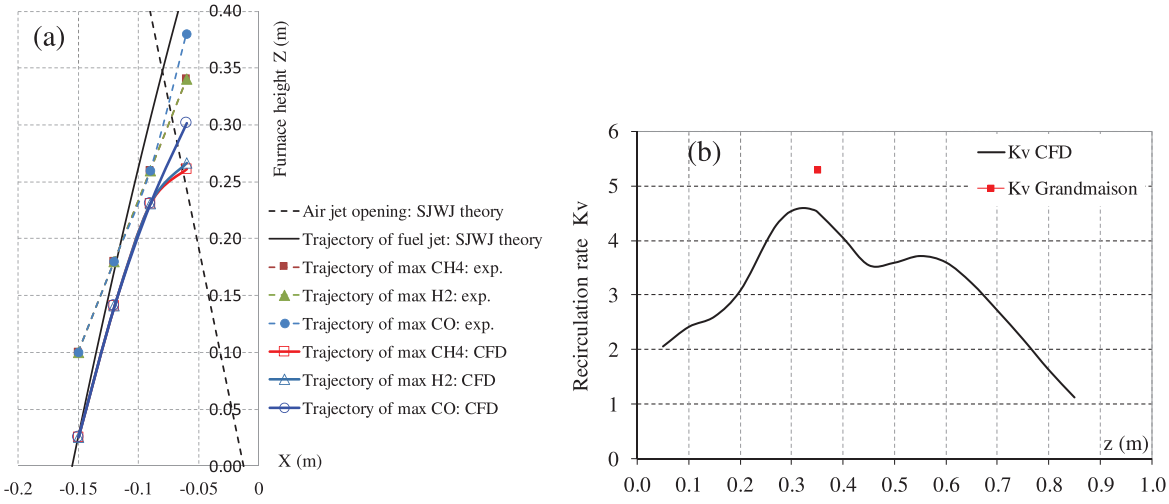

FIG. 4. (a) Trajectories of reactants jets: strong jet/weak jet (SJWJ) theory, experiment and CFD results. (b) Evolution of the recirculation rate along the furnace height z obtained from numerical simulation (black line), $K_v = 5.3$ calculated from the SJWJ theory (red symbol).

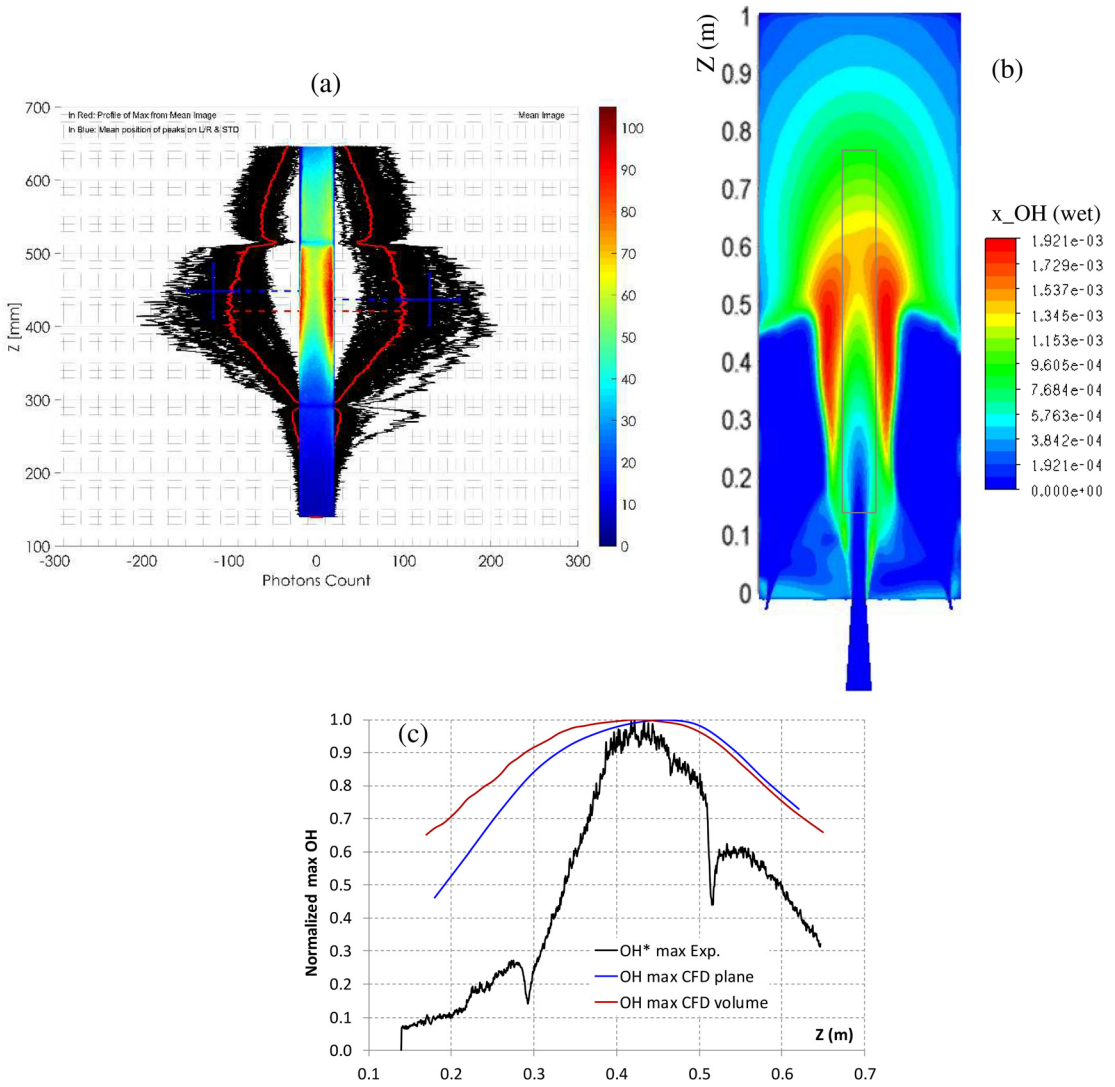

FIG. 5. (a) Experimental OH* radical chemiluminescence imaging. (b) OH mole fraction from CFD in the symmetrical plane. (c) Normalized maximum OH profiles; Exp.: considering the maximum of the averaged image of OH* photons count at each Z (black line). CFD: The maximum of (wet basis) OH mole fraction of each horizontal line (blue line) and each horizontal plane (red line) at each Z.

TABLE I. Energy balance and measurements at the furnace exit.

	Input (kW)	Output (kW)			Measurements at the furnace exit		
	Fuel power	Charge	Flue gas loss	Wall loss	Temperature (K)	CO_2 (vol. %-dry basis)	O_2 (vol. %-dry basis)
Experiment	30	17.16	8.96	3.88	1386	13.98	2.12
Simulation	30	16.97	8.98	4.05	1393	13.57	2.17

$$f = \sqrt{\left[1 - \frac{C_e^2 \ln(\eta)}{16\sqrt{\psi}}\right]^4 - \cos^2\theta}, \tag{13}$$

where ξ and η are the relative coordinates such as $\xi = z/d_{12}$ and $\eta = x/d_{12}$, respectively, d_{12} is the distance between the jets, C_e is the constant equal to 0.32, θ is the angle created by the injection axis of two jets, ψ is the ratio of impulse between two jets (impulse is the

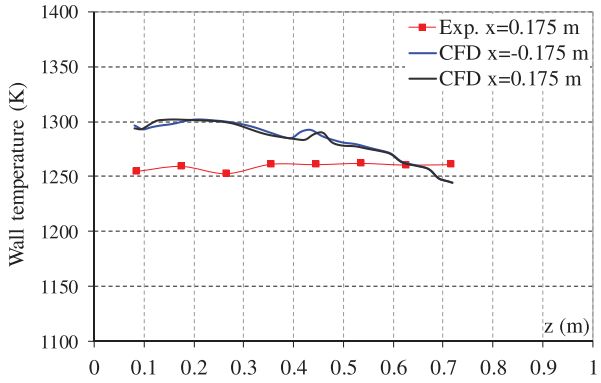

FIG. 6. Profiles of wall temperature along the furnace height obtained from experiment and simulation (CFD).

product of mass flow rate and bulk velocity), and x and z are the abscissa and ordinate as indicated in Fig. 1(c), respectively.

The evolution of maximum concentration of the three reactive species CH_4, H_2, and CO along the height in the symmetrical plane is displayed to visualize the fuel jet trajectories obtained experimentally and numerically. It is seen that, in experiment or in the simulation, the trajectories of max CH_4, H_2, and CO nearly collapse into each other, and the experimental and CFD fuel trajectories fairly follow the theoretical fuel trajectory until $z = 0.25$ m, after which they are bended toward the furnace axis. The intersection between the air jet opening and the fuel trajectories is called the confluence point, which is evaluated at $z = 0.35$ m for the SJWJ theory, which is considered as an upper limit, at $z = 0.3$ m for the experiment and between 0.25 and 0.3 m in the simulation.

The recirculated burnt gases flow rate is calculated from the simulation by determining, at each location z, the area portion for which the vertical velocity is negative. The recirculation rate, K_v, is then defined as the ratio between the recirculated burnt gases flow rate and the total inlet flow rate. The result of K_v is presented in Fig. 4(b). It is observed that K_v reaches the maximum value of 4.6 at $z = 0.32$ m slightly after the confluence point estimated at between $z = 0.25$ and 0.3 m. The value of K_v above four together with the furnace temperature above 1100 K (as be shown in the next section) fully satisfies the flameless combustion condition as expressed by Wünning and Wünning.[1] The recirculation rate can also be estimated using the Grandmaison's SJWJ theory[56]

$$K_v^{SJWJ} = \frac{t_{air,\xi}\, q_{air} + t_{fuel,\xi}\, q_{fuel}}{q_{air} + q_{fuel}}, \tag{14}$$

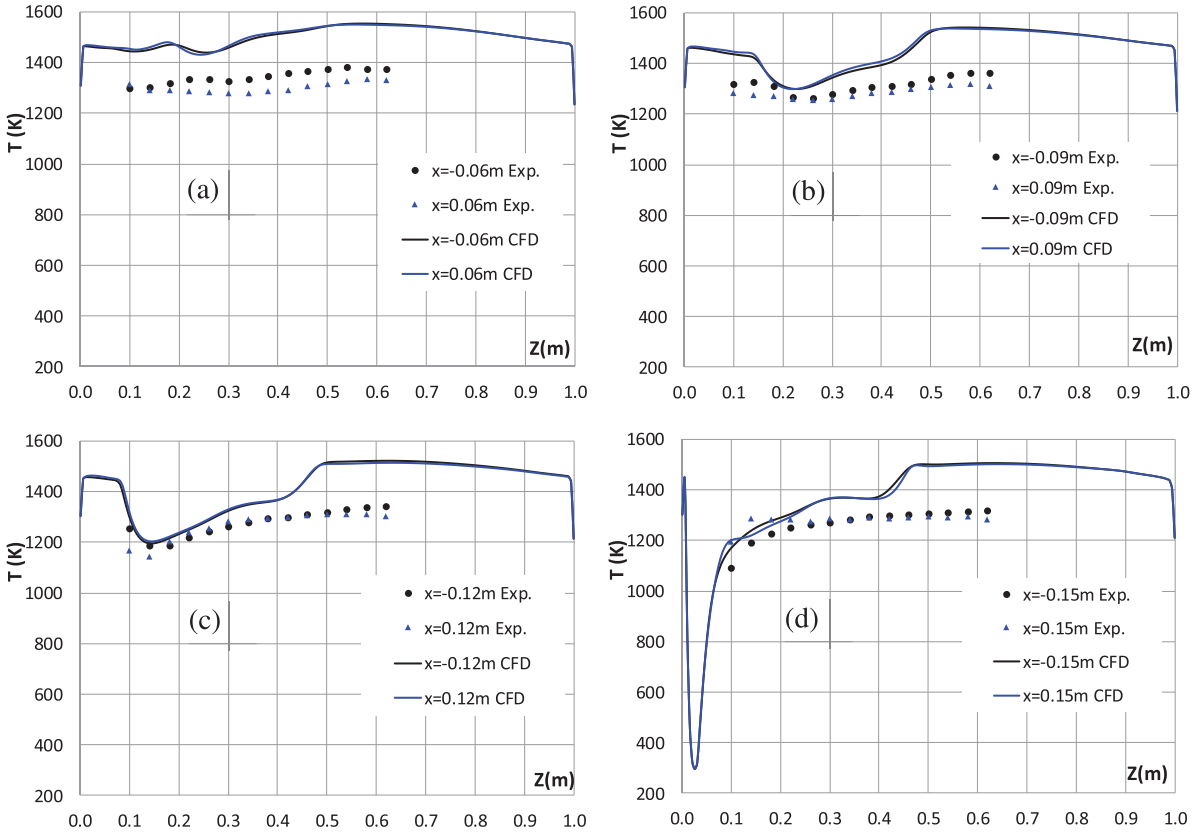

FIG. 7. Comparison between the experimental and computed profiles of temperature obtained at different (negative and positive) x positions and along the furnace height z. (a) $x = \pm 0.06$ m, (b) $x = \pm 0.09$ m, (c) $x = \pm 0.12$ m, and (d) $x = \pm 0.15$ m. Maximum measurement uncertainty is 7.6 K.

where q is the mass flow rate, $t_{air,\xi}$ and $t_{fuel,\xi}$ are the rates of entrainment of burnt gases by the air and fuel jets, respectively, which are calculated as follows:

$$t_{air,\xi} = C_e \frac{d_{12}}{d_{air,s}} \xi - 1, \tag{15}$$

$$t_{fuel,\xi} = \frac{C_e}{\cos\theta} \frac{d_{12}}{d_{fuel,s}} \int_0^{\xi} \left(1 - \frac{C_e^2 \ln(\eta)}{16\sqrt{\psi}}\right)^3 d\xi - 1, \tag{16}$$

where $d_{air,s}$ and $d_{fuel,s}$ are the effective diameters of the air and fuel jets in the exit section, respectively, which are given by $d\sqrt{\rho_0/\rho_\infty}$ (ρ_0, ρ_∞ are the densities of the jet in the exit section and of the surrounding fluid, respectively). The result of $K_v^{SJWJ} = 5.3$ at z = 0.35 m is also reported in Fig. 4(b). The interest of the SJWJ theory is to obtain a quick estimation of the recirculation rate at the confluence point by considering only flowrates of reactants and burner geometry. This can be used to give first burner sizing for new design or modification of existing design.

The reaction zone is experimentally visualized by OH* chemiluminescence imaging. OH* represents a good indicator of the reaction zone, and its emission is at 308 nm in UV,[34] a spectral region where the contribution of wall emission is negligible. Fifty instantaneous OH* images were recorded by the intensified camera (OH* images integrated over the depth of the furnace) and processed to get an average. Figure 5 shows the experimental result of OH* imaging, the contour of OH mole fraction obtained from the simulation, and the normalized maximum OH profiles obtained from both experiment and simulation. The contour of OH* [expressed in photons count, Fig. 5(a)] is the averaged image, the solid red profile was extracted from the maximum photons count on each horizontal line of the averaged image, and the maximum location is marked by the dashed red line. The black profiles were extracted from the maximum photons count on each horizontal line of the instantaneous image, and the blue crosses represent maximum photons count and its location with the corresponding standard deviations. The main reaction zones fluctuate with their peak locations varying from 0.40 to 0.49 m.

The frame in Fig. 5(b) corresponds to the optical window dimension, i.e., the frame of the contour of OH* photons count in Fig. 5(a). It is observed that the shape of the reaction zone is well captured by the simulation with one reaction zone stabilized on each side of the furnace axis. Figure 5(c) shows the experimental OH* peak at the location of z = 0.42 m. The simulation predicted the location of the maximum OH mole fraction at z = 0.46 m considering the OH distribution in the vertical symmetrical plane (CFD plane) and at z = 0.43 m when the distribution of OH in the whole volume is considered (CFD volume). It can be said that, by considering whole volume as it is the case with experimental OH* chemiluminescence, the simulation shows a good prediction of the location of the OH peak; the form and the location of the reaction zone are well recovered.

Table I compares the energy terms and the measurements at the furnace exit between the experiment and the simulation. It is noticed that the air preheating power was subtracted from the flue gas loss in

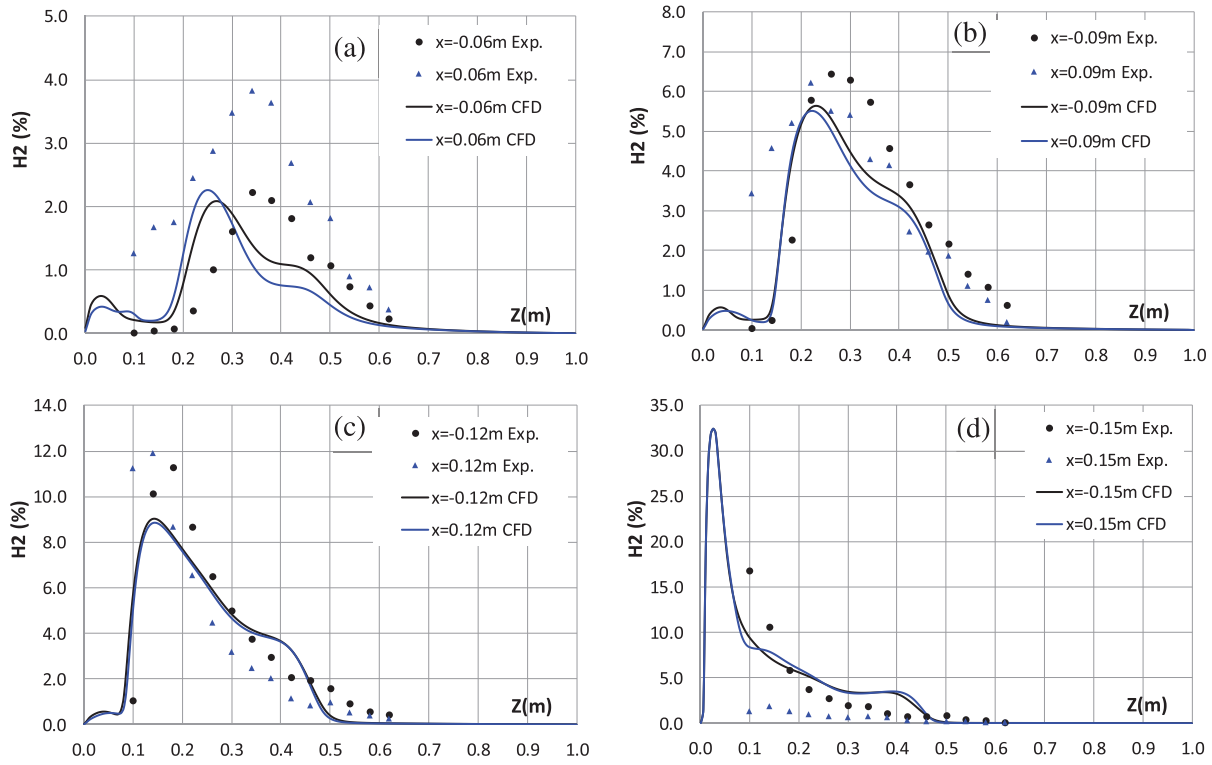

FIG. 8. Comparison between the experimental and computed profiles of H_2 in volume percentage on dry basis, obtained at different (negative and positive) x positions and along the furnace height z. (a) x = ±0.06 m, (b) x = ±0.09 m, (c) x = ±0.12 m, and (d) x = ±0.15 m. Maximum measurement uncertainty is 0.72%.

order to consider the fuel power as a single input. (This would be the case if the air were preheated by the flue gases as in an industrial regenerative burner.) The numerical simulation is able to reproduce the different terms measured experimentally, confirming the closure of the energy balance. 57% of the power input is transferred to the thermal charge and 80% of which is transferred by radiation and 20% by convection. This result confirms that the modeling of radiative properties based on the SLWSGG approach is able to predict correctly the heat transfer dominated by the radiation. Table I also shows the comparison for temperature and CO_2 and O_2 contents at the furnace exit between the experiment and the simulation with good agreement, validating the mass balance.

C. Comparison of numerical results with in-furnace measurements

Figure 6 compares the evolution of the vertical furnace wall temperature obtained from the experimental measurement and the simulation at the level of the symmetrical plane. The simulation provides an acceptable prediction; in average, the numerical result overpredicts only by 25 K the experimental value. It is also noted that the furnace wall temperature is always higher than 1250 K, a temperature value above which flameless combustion occurs. The variation of the wall temperature does not exceed 60 K in the experiment and in the simulation, confirming relatively good homogenization of temperature observed in the combustion chamber.

Figure 7 shows the comparison for the temperature between the measurement and the simulation results. Both the experimental and numerical results show rather flat temperature profiles; this is a characteristic of flameless combustion in which the temperature field is quasi-homogeneous and distributed largely in the whole volume, and local hot spots related to flames were not observed. The simulation overpredicts the experimental profiles by about 9%–14%. It is observed, at the locations of $x = \pm 0.12$ and ± 0.15 m, that the measured temperature decreases in the vicinity of the fuel jet, and this trend is well recovered by the simulation. The over-prediction of the temperature in highly diluted zones, where local extinctions and high fluctuations occur at $x = \pm 0.06$ m, may be attributed to the EDC turbulence chemistry interaction modeling. Christo and Dally[37] also found the same trend for the simulation of the most diluted case, the lowest 3% oxygen level in a hot co-flow, using EDC with the detailed chemistry GRI-3.0.[50] Discussions to improve temperature prediction by modifying or calculating directly volume fraction and residence time constants of species in fine structures based on local flow characteristics can be found in Refs. 42–45. This is beyond the scope of this work, which focuses on the implementation of the radiative properties model. Overall, the results obtained confirm that the integration of the radiative properties' SLWSGG model into the simulation provides a

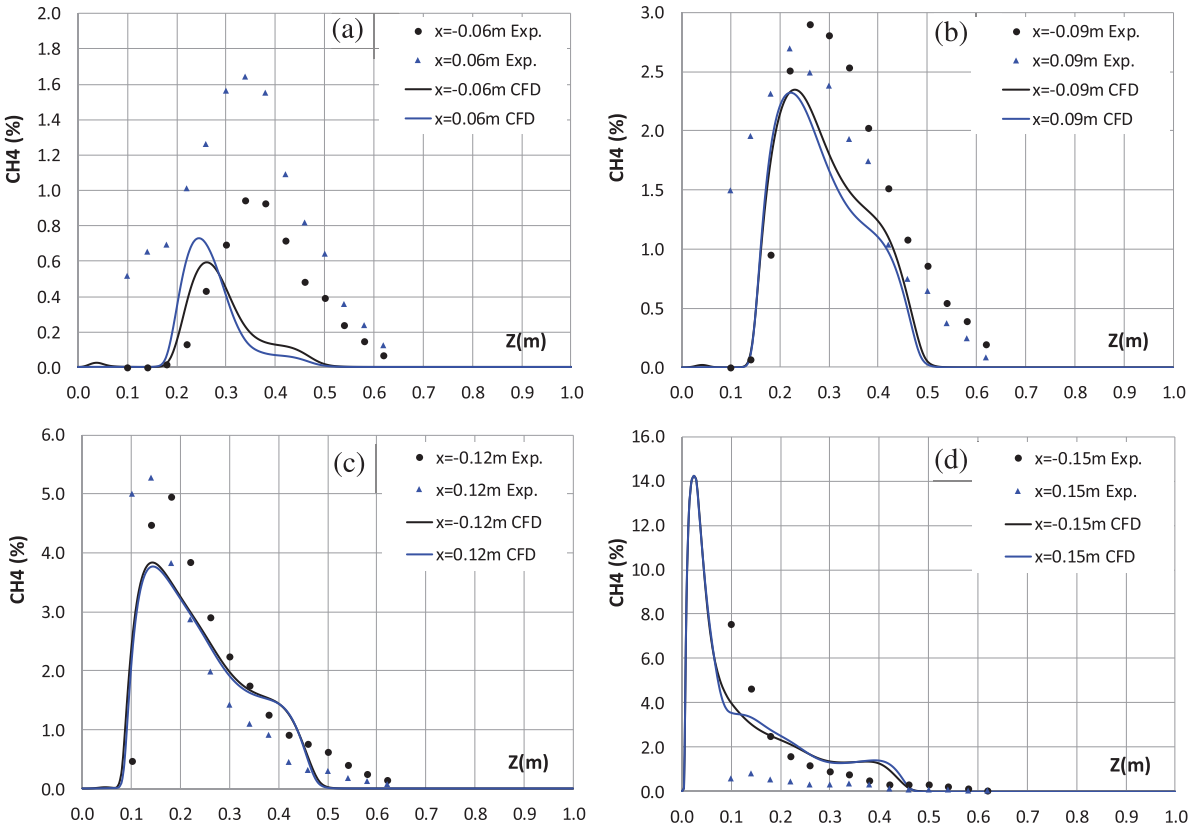

FIG. 9. Comparison between the experimental and computed profiles of CH_4 in volume percentage on dry basis, obtained at different (negative and positive) x positions and along the furnace height z. (a) $x = \pm 0.06$ m, (b) $x = \pm 0.09$ m, (c) $x = \pm 0.12$ m, and (d) $x = \pm 0.15$ m. Maximum measurement uncertainty is 0.27%.

reasonable prediction of the temperature level and trend in the context of flameless combustion simulation.

Figures 8–10 show the comparison between the measurement and the simulation results for three reactive species present in the fuel, namely, H_2, CH_4, and CO. The peak in each profile corresponds to the fuel jet, and these peaks are decreasing due to the mixing with the recirculated burnt gases and the air when moving farther from the fuel injector located at $x = \pm 0.155$ m. The measured species profiles at the location of $x = \pm 0.15$ m indicate a significant asymmetry of the fuel jet while the numerical results show rather symmetrical profiles for all locations. The computed species profiles at $x = \pm 0.15$ m agree only with the measured species profile at $x = -0.15$ m. As indicated by the experimental profiles at $x = +0.15$m, the content of three reactive species (H_2, CH_4, and CO) is very low in the vicinity of the fuel jet on the side of positive abscissa [the right side in Fig. 1(c)] where the sampling probe was introduced into the furnace. It could be possible that the interaction between the sampling probe and the fuel jet plays a role in such a phenomenon; the upstream of the sampling point in the fuel jet is perturbed by the probe while it is not the case for the side of negative abscissa.

The measurements show a farther penetration of the fuel jets in the flow field as compared to the results obtained from the simulation; higher peaks in the experimental species profiles are observed for all locations except $x = \pm 0.15$ m. The shapes of the profiles of the two reactive species H_2 and CH_4 are quite similar while the CO profiles appear to be wider particularly at $x = \pm 0.06$ m, because CO is not only the fuel species but also the intermediate minor species formed from oxidation of CH_4. The latest point is quite clear from the simulation profiles, as shown in Fig. 10; at $x = \pm 0.06$ m, the CO profiles are rather flat between $z = 0.2$ and 0.5 m where oxidation occurs, and there is contribution of CO intermediately produced. Overall, most of the expected levels, shapes, and trends observed in experiment are captured by the numerical results.

Figure 11 shows the comparison between the measurement and the simulation results for the oxidizer O_2 and the combustion product CO_2. It is noted that the distribution of oxygen is not symmetrical between the two measured O_2 profiles at $x = +0.09$ m and $x = -0.09$ m while it is not the case for the predicted O_2 profiles. The experimental trend of the measured O_2 profiles at $x = \pm 0.12$ m is not fully recovered by the simulation. As far as the profiles of CO_2 are concerned, the distribution is quite homogeneous, and the level is always higher than 13% (by volume), confirming that the combustion is highly diluted by the combustion products. The prediction of CO_2 can be seen acceptable as compared to the measurement.

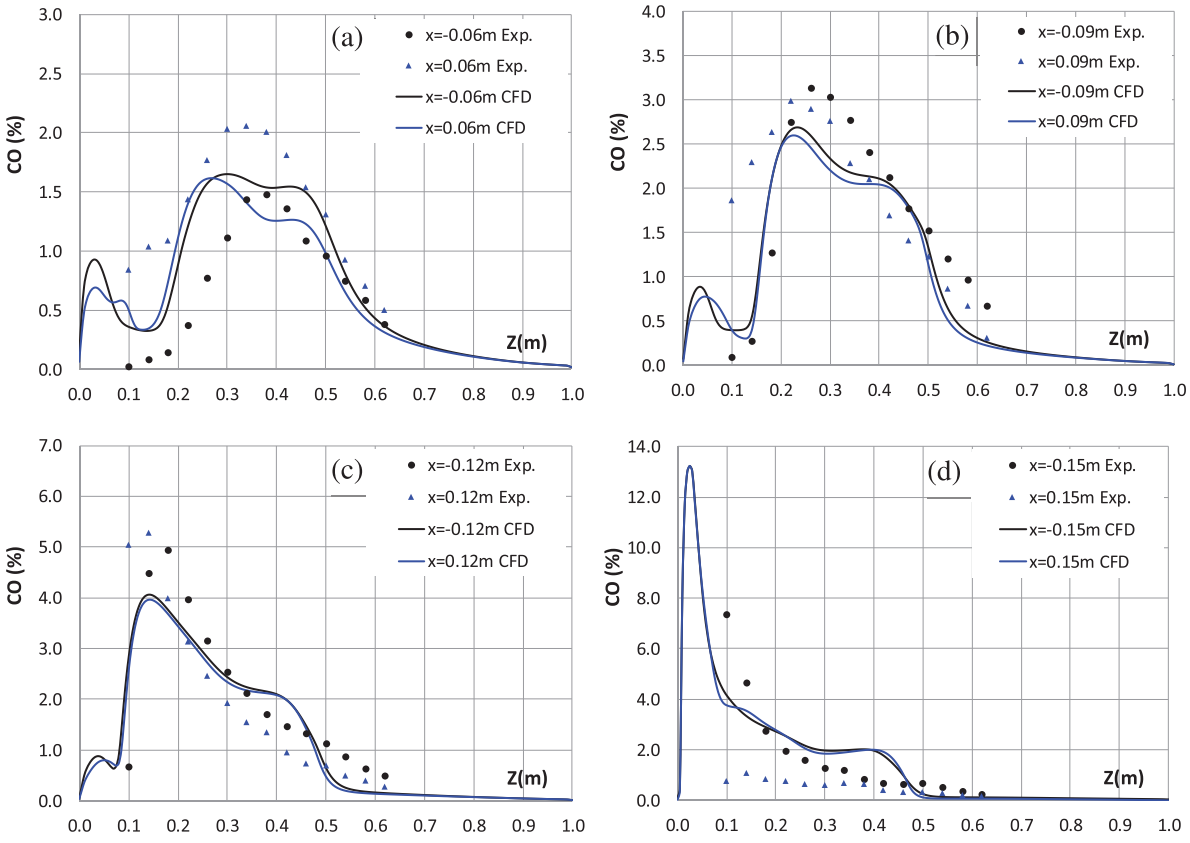

FIG. 10. Comparison between the experimental and computed profiles of CO in volume percentage on dry basis, obtained at different (negative and positive) x positions and along the furnace height z. (a) $x = \pm 0.06$ m, (b) $x = \pm 0.09$ m, (c) $x = \pm 0.12$ m, and (d) $x = \pm 0.15$ m. Maximum measurement uncertainty is 0.28%.

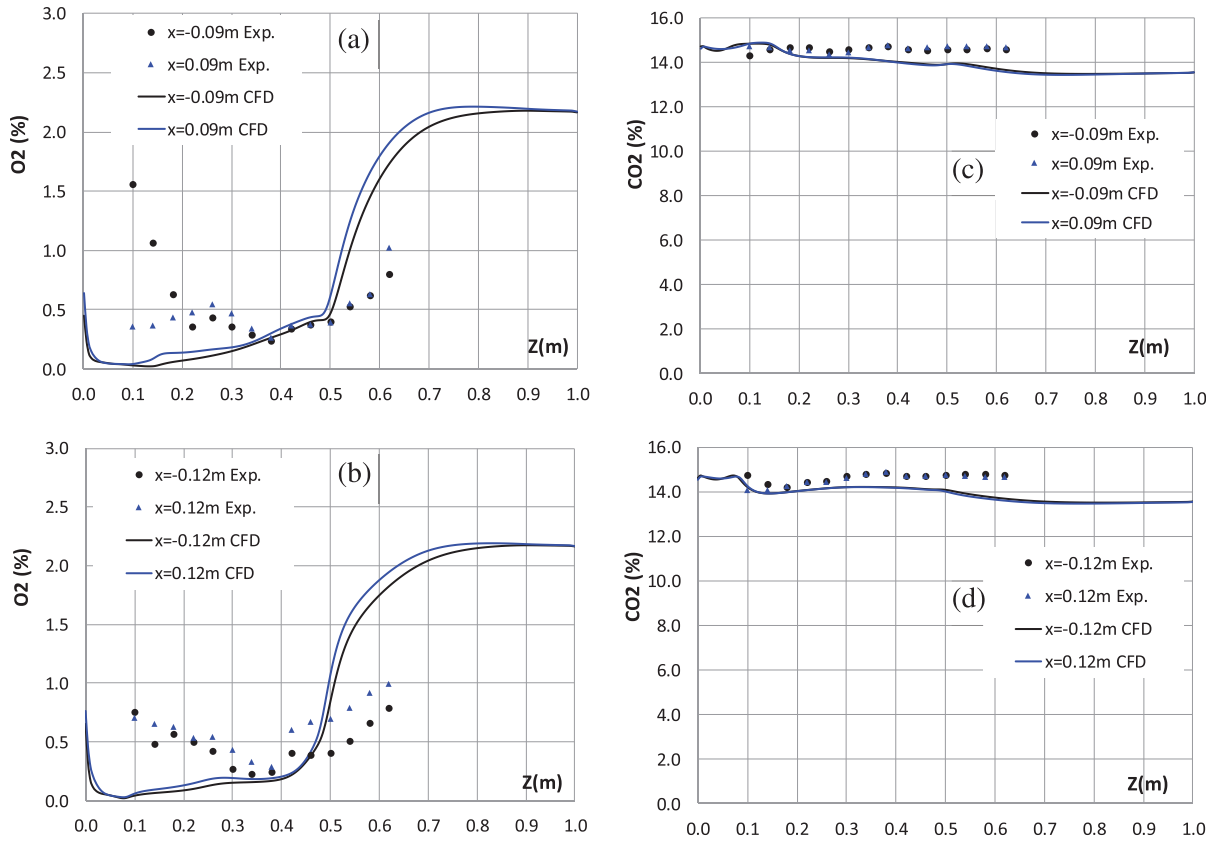

FIG. 11. Comparison between the experimental and computed profiles of O_2 and CO_2 in volume percentage on dry basis, obtained at two (negative and positive) x positions and along the furnace height z. (a) $x = \pm 0.09$ m and (b) $x = \pm 0.12$ m for O_2 and (c) $x = \pm 0.09$ m and (d) $x = \pm 0.12$ m for CO_2. Maximum measurement uncertainty is 0.35% and 0.85% for O_2 and CO_2, respectively.

IV. CONCLUSIONS AND PERSPECTIVES

A comprehensive modeling approach was proposed to model flameless combustion of low calorific value gases in which gaseous radiative properties were modeled with the spectral line-based weighted-sum-of-gray-gases (SLWSGG) approach. The emissivity weights and absorption coefficients were evaluated using the correlation of the line-by-line spectra of H_2O and CO_2 and optimized for a range of optical thicknesses and temperatures encountered in the considered furnace. The development of an experimental dataset of the combustion of a low calorific value syngas in a pilot furnace was used for the validation of the modeling approach. The furnace operates under flameless combustion, and the radiation is the dominant mode of heat transfer. The comparison between the simulation and the experiment confirms the need for such comprehensive modeling in the combustion system; heat transfer, energy balance, temperature, and chemical species fields were fairly predicted by the simulation.

This promising approach provides an interesting framework for comprehensive combustion modeling, which can include soot and NOx formation featuring strong interactions with radiative heat transfers. The discussed methodology can be easily extended to multiple fuel injection systems and to the combustion of green hydrogen or ammonia, which has gained much interest in research and industry decarbonization. The gas radiative properties can be calculated using spectroscopic databases presented under a lookup table, which may yield more accuracy than correlations.[57,58] Another perspective is also opening regarding the development of the reduced order model or digital twins using machine learning techniques. Each physical phenomenon should then be described in the framework of comprehensive multi-physics modeling to secure the production of large reliable databases for training of these machine learning based models.

ACKNOWLEDGMENTS

This paper was prepared to honor Professor Michael Pfitzner for his inspiring and seminal works on the modeling of complex combustion systems. H.-T.N. is funded by Agence Nationale de la Recherche et de la Technologie (ANRT) and ArcelorMittal under CIFRE No. 2019/0056. The experiment of G.M. was funded by the Walloon Government and ArcelorMittal. The help in different experimental and numerical aspects of Dr. Delphine Lupant, Mrs. Patricia Evrard, Mr. Marcel Rustin, and Mr. Christophe Coetsier at the University of Mons is gratefully acknowledged.

AUTHOR DECLARATIONS

Conflict of Interest

The authors have no conflicts to disclose.

DATA AVAILABILITY

The data that support the findings of this study are available from the corresponding author upon reasonable request.

REFERENCES

[1]J. A. Wünning and J. G. Wünning, "Flameless oxidation to reduce thermal NO-formation," Prog. Energy Combust. Sci. **23**, 81–94 (1997).

[2]T. Hasegawa and R. Tanaka, "High temperature air combustion-revolution in combustion technology; Part I: New findings on high temperature air combustion," JSME Int. J. Ser. B **41**, 1079–1084 (1998).

[3]A. Cavaliere and M. de Joannon, "Mild combustion," Prog. Energy Combust. Sci. **30**, 329–366 (2004).

[4]M. K. Denison and B. W. Webb, "A spectral line-based weighted-sum-of-gray-gases model for arbitrary RTE solvers," J. Heat Transfer **115**, 1004–1012 (1993).

[5]V. P. Solovjov, D. Lemonnier, and B. W. Webb, "The SLW-1 model for efficient prediction of radiative transfer in high temperature gases," J. Quant. Spectrosc. Radiat. Transfer **112**(7), 1205–1212 (2011).

[6]P. Evrard, V. Feldheim, and P. Lybaert, "An alternative method to optimise the SLW grey gases," J. Phys. **395**, 012007 (2012).

[7]P.-D. Nguyen, A. Danda, M. Embouazza, M. Gazdallah, P. Evrard, and V. Feldheim, "Application of the spectral line-based weighted-sum-of-gray-gases model (SLWSGG) to the calculation of radiative heat transfer in steel reheating furnaces firing on low heating value gases," J. Phys. **369**, 012008 (2012).

[8]B. W. Webb, V. P. Solovjov, and F. André, "The spectral line weighted-sum-of-gray-gases (SLW) model for prediction of radiative transfer in molecular gases," in *Advances in Heat Transfer*, edited by E. M. Sparrow, J. P. Abraham, J. M. Gorman, and W. J. Minkowycz (Academic Press, New York, 2019), Vol. 51, pp. 207–298.

[9]M. K. Denison and B. W. Webb, "An absorption-line blackbody distribution function for efficient calculation of gas radiative transfer," J. Quant. Spectrosc. Radiat. Transfer **50**, 499–510 (1993).

[10]M. K. Denison and B. W. Webb, "Development and application of an absorption-line blackbody distribution function for CO_2," Int. J. Heat Mass Transfer **38**, 1813–1821 (1995).

[11]L. S. Rothman, C. Camy-Peyret, J.-M. Flaud, R. R. Gamache, A. Goldman, D. Goorvitch, R. L. Hawkins, J. Schroeder, J. E. A. Selby, and R. B. Wattson, http://www.hitran.com for "HITEMP, The High-Temperature Molecular Spectroscopic Database" (2000).

[12]S. A. Tashkun, V. I. Perevalov, A. D. Bykov, N. N. Lavrentieva, and J.-L. Teffo, ftp://ftp.iao.ru/pub/CDSD-1000 for "Carbon Dioxide Spectroscopic Databank (CDSD)" (2002).

[13]S. A. Tashkun, V. I. Perevalov, J.-L. Teffo, A. D. Bykov, and N. N. Lavrentieva, "CDSD-1000, the high temperature carbon dioxide spectroscopic databank," J. Quant. Spectrosc. Radiat. Transfer **82**(1–4), 165–196 (2003).

[14]M. F. Modest and R. S. Mehta, "Full spectrum k-distribution correlations for CO_2 from the CDSD-1000 spectroscopic databank," Int. J. Heat Mass Transfer **47**, 2487–2491 (2004).

[15]M. F. Modest and V. Singh, "Engineering correlations for full spectrum k-distributions of H_2O from the HITEMP spectroscopic databank," J. Quant. Spectrosc. Radiat. Transfer **93**, 263–271 (2005).

[16]B. B. Dally, A. N. Karpetis, and R. S. Barlow, "Structure of turbulent non-premixed jet flames in a diluted hot flow," Proc. Combust. Inst. **29**, 1147–1154 (2002).

[17]E. Oldenhof, M. J. Tummers, E. H. vanVeen, and D. Roekaerts, "Role of entrainment in the stabilisation of jet-in-hot-coflow flames," Combust. Flame **158**, 1553–1563 (2011).

[18]M. Ayoub, C. Rottier, S. Carpentier, C. Villermaux, A. M. Boukhalfa, and D. Honoré, "An experimental study of mild flameless combustion of methane/hydrogen mixtures," Int. J. Hydrogen Energy **37**, 6912–6921 (2012).

[19]D. Lupant, B. Pesenti, and P. Lybaert, "Influence of probe sampling on reacting species measurement in diluted combustion," Exp. Therm. Fluid Sci. **34**, 516–522 (2010).

[20]D. Lupant, "Caractérisation exp érimentale détaillée et modélisation numérique de la combustion diluée du gaz naturel sur une installation de laboratoire de 30kW," Ph.D. thesis (University of Mons, 2011).

[21]D. Lupant and P. Lybaert, "Assessment of the EDC combustion model in MILD conditions with in-furnace experimental data," Appl. Therm. Eng. **75**, 93–102 (2015).

[22]G. Mosca, D. Lupant, and P. Lybaert, "Effect of increasing load on the MILD combustion of COG and its blend in a 30 kW furnace using low air preheating temperature," Energy Proc. **120**, 262–269 (2017).

[23]G. Mosca, "Numerical and experimental study on MILD combustion of low LHV fuels," Ph.D. thesis (University of Mons, 2017).

[24]J. Badger, B. W. Webb, and V. P. Solovjov, "An exploration of advanced SLW modeling approaches in comprehensive combustion predictions," Combust. Sci. Technol. **194**, 225–241 (2022).

[25]F. Liu, J.-L. Consalvi, P. J. Coelho, F. Andre, M. Gu, V. Solovjov, and B. W. Webb, "The impact of radiative heat transfer in combustion processes and its modeling-with a focus on turbulent flames," Fuel **281**, 118555 (2020).

[26]L. Pierrot, P. Rivière, A. Soufiani, and J. Taine, "A fictitious-gas-based absorption distribution function global model for radiative transfer in hot gases," J. Quant. Spectrosc. Radiat. Transfer **62**, 609–624 (1999).

[27]M. F. Modest, *Radiative Heat Transfer*, 2nd ed. (McGraw-Hill, New York, 2003).

[28]A. A. Lacis and V. Oinas, "A description of the correlated-k distribution method for modelling nongray gaseous absorption, thermal emission, and multiple scattering in vertically inhomogeneous atmospheres," J. Geophys. Res. **96**, 9027–9063, https://doi.org/10.1029/90JD01945 (1991).

[29]W. A. Fiveland, "Discrete-ordinates solution of the radiative transport equation for rectangular enclosures," J. Heat Transfer **106**, 699–706 (1984).

[30]P. J. Coelho, "Numerical simulation of the interaction between turbulence and radiation in reactive flows," Prog. Energy Combust. Sci. **33**, 311–383 (2007).

[31]R. Johansson, K. Andersson, B. Leckner, and H. Thunman, "Models for gaseous radiative heat transfer applied to oxy-fuel conditions in boilers," Int. J. Heat Mass Transfer **53**(1–3), 220–230 (2010).

[32]A. Ziemniczak, R. Brittes, F. Cassol, and F. França, "Evaluation of the number of gray gases in the WSGG model," in Proceedings 22nd International Congress of Mechanical Engineering (COBEM 2013), Ribeirao Preto, SP, Brazil, 2013.

[33]ANSYS FLUENT theory and user guide. v19.4.

[34]L. C. Haber, "An investigation into the origin, measurement and application of chemiluminescent light emissions from premixed flames," Ph.D. thesis (VirginiaTech, 2000).

[35]H. C. Hottel and A. F. Sarofim, *Radiative Transfer* (McGraw-Hill, New York, 1967).

[36]B. W. Webb, V. P. Solovjov, and F. André, "An exploration of the influence of spectral model parameters on the accuracy of the rank correlated SLW model," J. Quant. Spectrosc. Radiat. Transfer **218**, 161–170 (2018).

[37]F. C. Christo and B. B. Dally, "Modeling turbulent reacting jets issuing into a hot and diluted coflow," Combust. Flame **142**, 117–129 (2005).

[38]S. A. Orszag, V. Yakhot, W. S. Flannery, F. Boysan, D. Choudhury, J. Maruzewski, and B. Patel, "Renormalization group modeling and turbulence simulations," in International Conference on Near-Wall Turbulent Flows, Tempe, Arizona, 1993.

[39]B. F. Magnussen, "On the structure of turbulence and generalized eddy dissipation concept for chemical reaction in turbulent flow," in 19th AIAA Aerospace Science Meeting (1981).

[40]I. R. Gran and B. F. Magnussen, "A numerical study of a bluff-body stabilized diffusion flame. Part 2. Influence of combustion modeling and finite-rate chemistry," Combust. Sci. Technol. **119**, 191–217 (1996).

[41]R. W. Bilger, S. H. Starner, and R. J. Kee, "On reduced mechanisms for methane-air combustion in nonpremixed flames," Combust. Flame **80**, 135–149 (1990).

[42]A. De, E. Oldenhof, P. Sathiah, and D. Roekaerts, "Numerical simulation of delft-jet-in-hot-coflow (DJHC) flames using the eddy dissipation concept

model for turbulence-chemistry interaction," Flow. Turbul. Combust. **87**, 537–567 (2011).
[43]J. Aminian, C. Galletti, S. Shahhosseini, and L. Tognotti, "Numerical investigation of a MILD combustion burner: Analysis of mixing field, chemical kinetics and turbulence-chemistry interaction," Flow. Turbul. Combust. **88**, 597–623 (2012).
[44]A. Parente, M. R. Malik, F. Contino, A. Cuoci, and B. B. Dally, "Extension of the eddy dissipation concept for turbulence/chemistry interactions to mild combustion," Fuel **163**, 98–111 (2016).
[45]N. Romero, H. Bao, X. Huang, K. Martin, and D. Roekaerts, "Simulation of flameless combustion in delft lab-scale furnace using EDC model," in Proceedings of the 9th European Combustion Meeting, 2019.
[46]T. Silei, G. Sorrentino, R. Ragucci, and C. Galletti, "Reaction-rate based modeling of MILD combustion in a cyclonic burner," in Proceedings of the 10th European Combustion Meeting, 2021.
[47]S. B. Pope, "Computationally efficient implementation of combustion chemistry using in situ adaptive tabulation," Combust. Theory Model. **1**, 41–63 (1997).
[48]C. Galletti, A. Parente, M. Derudi, R. Rota, and L. Tognotti, "Numerical and experimental analysis of NO emissions from a lab-scale burner fed with hydrogen-enriched fuels and operating in MILD combustion," Int. J. Hydrogen Energy **34**, 8339–8351 (2009).
[49]A. Parente, C. Galletti, and L. Tognotti, "A simplified approach for predicting NO formation in MILD combustion of CH_4-H_2 mixtures," Proc. Combust. Inst. **33**, 3343–3350 (2011).
[50]G. P. Smith, D. M. Golden, M. Frenklach, N. W. Moriarty, B. Eiteneer, M. Goldenberg, C. T. Bowman, R. K. Hanson, S. Song, W. C. Gardiner, Jr., V. V. Lissianski, and Z. Qin, see http://www.me.berkeley.edu/gri_mech/ for "GRI-Mech 3.0" (1999).
[51]A. Kazakov and M. Frenklach, see http://combustion.berkeley.edu/drm/ (last accessed December 09, 2020).
[52]M. Ferrarotti, W. De Paepe, and A. Parente, "Reactive structures and NO_x emissions of methane/hydrogen mixtures in flameless combustion," Int. J. Hydrogen Energy **46**, 34018–34045 (2021).
[53]X. Huang, M. J. Tummers, E. H. van Veen, and D. Roekaerts, "Modelling of MILD combustion in a lab-scale furnace with an extended FGM model including turbulence–radiation interaction," Combust. Flame **237**, 111634 (2022).
[54]A. Soufiani and E. Djavdan, "A comparison between weighted sum of gray gases and statistical narrow band radiation models for combustion applications," Combust. Flame **97**, 240–250 (1994).
[55]T. F. Smith, Z. F. Shen, and J. N. Friedman, "Evaluation of coefficients for the weighted sum of gray gases model," J. Heat Transfer **104**, 602–608 (1982).
[56]E. W. Grandmaison, I. Yimer, H. A. Becker, and A. Sobiesiak, "The strong jet/weak jet problem and aerodynamic modeling of the CGRI burner," Combust. Flame **114**, 381–396 (1998).
[57]J. Pearson, B. W. Webb, V. P. Solovjov, and J. Ma, "Updated correlation of the absorption-line blackbody distribution function for H_2O based on the HITEMP2010 database," J. Quant. Spectrosc. Radiat. Transfer **128**, 10–17 (2013).
[58]J. Pearson, B. W. Webb, V. P. Solovjov, and J. Ma, "Efficient representation of the absorption line blackbody distribution function for H_2O, CO_2, and CO at variable temperature, mole fraction, and total pressure," J. Quant. Spectrosc. Radiat. Transfer **138**, 82–96 (2014).